JCI insight

Tissue-localized immune responses in people with cystic fibrosis and respiratory nontuberculous mycobacteria infection

Don Hayes Jr., … , Namal P.M. Liyanage, Richard T. Robinson

JCI Insight. 2022;7(12):e157865. https://doi.org/10.1172/jci.insight.157865.

Research Article | Infectious disease | Pulmonology

Graphical abstract

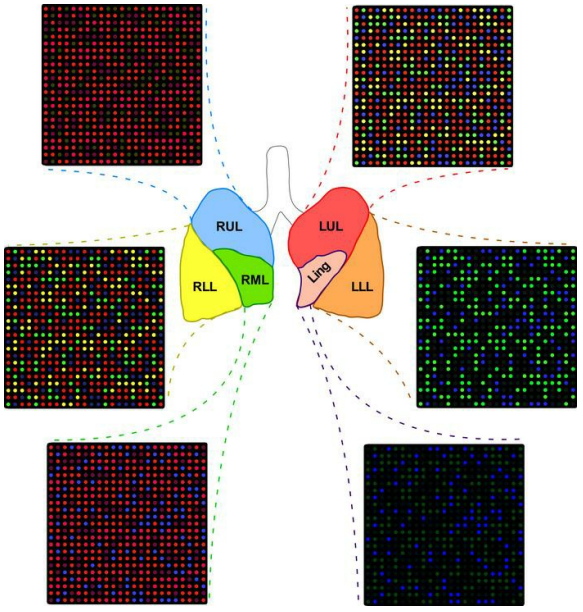

Find the latest version:

https://jci.me/157865/pdf

JCI insight

RESEARCH ARTICLE

Tissue-localized immune responses in people with cystic fibrosis and respiratory nontuberculous mycobacteria infection

Don Hayes Jr.,[1] Rajni Kant Shukla,[2] Yizi Cheng,[1] Emrah Gecili,[1] Marlena R. Merling,[2] Rhonda D. Szczesniak,[1] Assem G. Ziady,[1] Jason C. Woods,[1] Luanne Hall-Stoodley,[2] Namal P.M. Liyanage,[2] and Richard T. Robinson[2]

[1]Cincinnati Children's Hospital Medical Center, Department of Pediatrics, University of Cincinnati College of Medicine, Cincinnati, Ohio, USA. [2]Department of Microbial Infection and Immunity, The Ohio State University, Columbus, Ohio, USA.

Nontuberculous mycobacteria (NTM) are an increasingly common cause of respiratory infection in people with cystic fibrosis (PwCF). Relative to those with no history of NTM infection (CF-NTM^{NEG}), PwCF and a history of NTM infection (CF-NTM^{POS}) are more likely to develop severe lung disease and experience complications over the course of treatment. In other mycobacterial infections (e.g., tuberculosis), an overexuberant immune response causes pathology and compromises organ function; however, since the immune profiles of CF-NTM^{POS} and CF-NTM^{NEG} airways are largely unexplored, it is unknown which, if any, immune responses distinguish these cohorts or concentrate in damaged tissues. Here, we evaluated lung lobe–specific immune profiles of 3 cohorts (CF-NTM^{POS}, CF-NTM^{NEG}, and non-CF adults) and found that CF-NTM^{POS} airways are distinguished by a hyperinflammatory cytokine profile. Importantly, the CF-NTM^{POS} airway immune profile was dominated by B cells, classical macrophages, and the cytokines that support their accumulation. These and other immunological differences between cohorts, including the near absence of NK cells and complement pathway members, were enriched in the most damaged lung lobes. The implications of these findings for our understanding of lung disease in PwCF are discussed, as are how they may inform the development of host-directed therapies to improve NTM disease treatment.

Introduction

Cystic fibrosis (CF) is caused by mutations in the cystic fibrosis transmembrane conductance regulator (*CFTR*) gene that cause airway surface liquid dehydration and the accumulation of mucus, which can obstruct airways and reduce lung function (1). The quality of life and life expectancy of people with CF (PwCF) are improved by therapies that modulate *CFTR* function or replace the lungs entirely (i.e., lung transplant, LTX); nevertheless, the median life expectancy of PwCF is still only 40 years of age (2). Chronic respiratory infections (CRI) further shorten the median life span of PwCF and can preclude them from lung transplant eligibility (3–5). Therefore, it is important to identify factors that can be manipulated via host-directed therapies (HDTs) to prevent or improve CRI outcomes in PwCF.

Nontuberculous mycobacteria (NTM) are an increasingly common cause of CRIs in PwCF (6–10). *Mycobacterium avium* or *M. abscessus* complex members cause most respiratory NTM infections (11). The route by which they enter the lung, however, is often not clear; possibilities include inhalation exposure to environmental aerosols (12), silent aspiration (since NTM infections have been associated with gastroesophageal reflux disease) (13), or carryover from contaminated bronchoscopes (14). Once in the lung, NTM become intracellular and replicate within the phagosome of innate immune lineages, e.g., macrophages (MØ); they are also capable of forming biofilms (15, 16). PwCF who are infected with NTM (i.e., individuals who are CF-NTM^{POS}) typically suffer more severe lung disease than those without NTM infection (i.e., individuals who are CF-NTM^{NEG}) (11), and numerous case reports suggest that pre-LTX infection with NTM is indicative of morbidity following LTX or allograft dysfunction (11, 17–21). Estimates of NTM infection prevalence within the CF community range from 3%–23% and vary based on microbiological criteria and country (4). The reason(s) why individuals who are CF-NTM^{POS} are more prone to experiencing complications during CF treatment or following LTX are unknown.

Authorship note: DH and RKS contributed equally to this work. NPML and RTR are co–corresponding authors.

Conflict of interest: The authors have declared that no conflict of interest exists.

Submitted: December 22, 2021
Accepted: April 29, 2022
Published: June 22, 2022

Reference information: *JCI Insight*. 2022;7(12):e157865. https://doi.org/10.1172/jci.insight.157865.

In animal models of mycobacterial disease, the local immune environment greatly affects lung disease progression and antibiotic treatment efficacy (22). On one end of the spectrum, the absence of an immune response — whether due to impaired bactericidal activity on the part of MØ or diminished secretion of MØ-activating cytokines by T cells — enables unrestricted mycobacterial growth. On the other end of the spectrum, an overexuberant response by innate or adaptive lineages can lead to tissue damage, fibrosis, and compromised lung function. Whether the immune profile of CF-NTM^{POS} lungs is best characterized as absent or overexuberant is not known, nor is it known if CF-NTM^{POS} lungs have immunological features that distinguish them from CF-NTM^{NEG} lungs. This is an important distinction from a translational perspective, as our ability to modulate inflammation continues to improve with the advent of biologics that enhance or suppress the activity of specific cells or cytokines. To date, the only biologics that have been tested in clinical trials as HDTs for respiratory NTM infection are inhaled forms of recombinant GM-CSF (23) and recombinant IFNγ (24, 25), each being well tolerated but nevertheless limited in their mycobactericidal efficacy compared with placebo controls (26, 27). Should there be immune factors that drive CF-NTM^{POS} lung pathology, it may be possible to use biologics as HDTs to improve antimycobacterial therapy in PwCF.

To profile the immune response and its biogeographical distribution in CF-NTM^{POS} lungs, we performed a cross-sectional study of 3 cohorts: individuals who are CF-NTM^{POS}, individuals who are CF-NTM^{NEG}, and control individuals without CF (CTRL). Lung lobe–specific radiological assessments, bronchoalveolar lavage fluid (BALF) samples and blood were collected from each cohort and the frequencies of multiple innate and adaptive immune lineages were determined, as were lobe-specific protein concentrations of multiple cytokines and complement pathway members. Our results indicate a number of immunological differences between CF-NTM^{POS} and CF-NTM^{NEG} lungs, many of which are lung-specific and concentrated in the most damaged lobes. We also observed a number of heretofore unreported differences between CTRL and CF individuals that may influence the general susceptibility of PwCF to opportunistic pathogens, as well as lobe-specific differences that support a perspective wherein the lung is not a uniform environment but rather is a conglomerate of immunologically distinct biogeographical regions.

Results

CF-NTM^{POS} lungs exhibit more tissue damage that is concentrated in the right and upper lobes

To profile the immune response and its biogeographical distribution within CF-NTM^{NEG} and CF-NTM^{POS} lungs, BALF and blood from individuals who are CF-NTM^{NEG} and CF-NTM^{POS} were collected during clinically indicated bronchoscopies and used for multidimensional flow cytometry analysis and cytokine protein measurements. Clinical lung function measurements (forced expiratory volume in 1 second [FEV_1], forced vital capacity [FVC]) and lobe-specific radiological assessments (CT) were made prior to BALF collection. To establish baseline cell and cytokine levels in the absence of CF, BALF and blood were collected in an identical manner from an additional CTRL cohort. The physical characteristics of each cohort are shown in Table 1, along with aggregate clinical microbiology data (BALF culture), demonstrating that the presence of common opportunistic pathogens (*S. aureus*, *P. aeruginosa*, *Aspergillus,* and *Candida* spp) was similar between CF-NTM^{NEG} and CF-NTM^{POS} cohorts. *M. abscessus* and *M. intracellulare*/*M. chimaera* were the species present in CF-NTM^{POS} subjects. Clinical microbiology data at the individual level are provided in Supplemental Table 1 (supplemental material available online with this article; https://doi.org/10.1172/jci.insight.157865DS1). Per our experimental design (Figure 1), BALF samples from the right lung lobes — right upper lobe (RUL), right middle lobe (RML), and right left lobe (RLL) — of each individual were collected and kept separate at the time of bronchoscopy, as were BALF samples from the left lung lobes — left upper lobe (LUL), lingula (Ling), and left lower lobe (LLL).

As shown in Figure 2, A and B, the FEV_1 and FVC measurements from our CF-NTM^{NEG} and CF-NTM^{POS} cohorts are consistent with their both having compromised lung function. With regards to the nature and distribution of tissue damage, however, CT scans of the same individuals demonstrated that a higher proportion of CF-NTM^{POS} lungs exhibited moderate bronchiectasis, mucus plugging, and bronchial wall thickening, each of which was concentrated in right and upper lobes (Figure 2C and Supplemental Figure 1). CF-NTM^{POS} lungs were also the only ones in which cysts were observed (Figure 2C and Supplemental Figure 1). Neither individuals who are CF-NTM^{NEG} nor CF-NTM^{POS} exhibited cavitary lung lesions. Consistent with CF-NTM^{POS} lungs having more tissue damage, there were significantly more cells in BALF from CF-NTM^{POS} lungs (Figure 2D), with the majority of cells being CD45^{NEG} (Figure 2E) and dead (Figure 2F).

Table 1. The clinical characteristics of our study subjects

Cohort	Total	Age (Avg)	Female:Male	BMI (Avg)	*CFTR* genotypes	SA	PA	Fungi	NTM
CTRL	7	20–39 yrs (27)	4:3	20.1–34.3 (25.2)	Undetermined				
CF-NTM^{NEG}	7	19–36 yrs (24.4)	5:2	18.9–28.2 (23.9)	F508del/F508del (5) F508del/R553X (1) F508del/N1303K (1)	4/7	5/7	3/7	Not detected
CF-NTM^{POS}	4	20–32 yrs (24.8)	2:2	15.7–26.2 (22)	F508del/F508del (2) F508del/c221delG (1) F508del/4077-4080delTGTTinsAA (1)	1/4	1/4	2/4	*M. abscessus* (3) *M. intracellulare* / *M. chimaera* (1)

Adult subjects were divided into 1 of 3 cohorts based on their CF status and NTM infection history: CTRL, healthy individuals without CF; CF-NTM^{NEG}, individuals with CF but no history of NTM infection; and CF-NTM^{POS}, individuals with CF and a history of NTM infection. Listed are aggregate data regarding the total number of individuals per cohort, their age range, female/male ratio, BMI, the *CFTR* genotypes represented, and the clinical microbiology results of BALF specimens. Clinical microbiology results are presented as the portion of individuals who were positive for the indicated microbe (SA, *S. aureus*; PA, *P. aeruginosa*; Fungi: *Aspergillus* or *Candida* spp), and in the case of individuals who are CF-NTM^{POS}, which *Mycobacteria* species were present. Individual clinical microbiology data are provided in Supplemental Table 1.

CF-NTM^{POS} airways are distinguished by changes in multiple innate and adaptive immune lineage frequencies

Since tissue damage is often accompanied by changes in the local immune environment, we used multidimensional flow cytometry to determine the frequencies of adaptive and innate immune lineages (live CD45^{POS} cells) in right lung BALF and left lung BALF as well as in the blood of CTRL and individuals who are both CF-NTM^{NEG} and CF-NTM^{POS}. t-distributed stochastic embedding (t-SNE) analysis of the cumulative data from each individual indicated that the airways have multiple populations with staining characteristics that are consistent with a number of conventional immune subsets (e.g., T cells, MØs) as well as several unexpected subsets, e.g., double-negative (DN) T cells (Figure 3A). Conventional flow analysis using the gating scheme shown in Supplemental Figure 2 was used to quantify the relative abundance of each subset in the airway (Figure 3, B–P) and in the blood (Figure 4) to determine if any differences were tissue specific.

There were several notable differences between cohorts with respect to adaptive immune lineages (Figure 3, B–H). First, relative to CTRL and CF-NTM^{NEG} airways, CF-NTM^{POS} airways had significantly higher frequencies of B cells (Figure 3B). This was unexpected given the historical view of B cells as being disassociated from mycobacterial disease resistance. Second, CF-NTM^{NEG} and CF-NTM^{POS} cohorts each had significantly lower frequencies of CD4 T cells in the airways, relative to CTRL (Figure 3C), whereas airway CD8 T cell frequencies were similar across all cohorts (Figure 3D). Net declines in the CD4:CD8 ratio stemmed from this drop in CD4 T cell frequency and were observed in both PwCF cohorts (Figure 3H). Third and unexpectedly, we observed 2 T cell populations in the airways that typically associate with thymic development: CD4^{+}CD8^{+} double-positive (DP) T cells (Figure 3F) and CD4^{-}CD8^{-} DN T cells (Figure 3G). Both PwCF cohorts had higher and lower frequencies of DP and DN T cells, respectively, compared with our CTRL cohort. Most of the above differences in adaptive lineage frequencies were specific to the lung and were not seen in the blood (Figure 4, A–H).

There were also notable differences between cohorts with respect to innate lineages in the airway (Figure 3, I–P). Relative to the CTRL cohort, the CF-NTM^{NEG} and CF-NTM^{POS} cohorts had lower frequencies of airway NK cells, with CF-NTM^{POS} levels being lowest and significantly below those of CF-NTM^{NEG} (Figure 3I). Conversely, airway group 1 innate lymphoid cell (ILC1) — which are developmentally related to NK cells — were increased in the CF-NTM^{POS} cohort relative to CTRL (Figure 3J). The frequencies of airway ILC2, ILC3 NCR^{+}, and ILC3 NCR^{-} were similar across all cohorts (Figure 3, K–M), as were airway NKT cells (Figure 3E). Among phagocytic subsets, the frequency of classical MØ/monocytes was significantly higher in the CF-NTM^{POS} cohort relative to CF-NTM^{NEG} and CTRL (Figure 3N). Decreased frequencies of intermediate MØ/monocytes were observed in CF-NTM^{NEG} and CF-NTM^{POS} cohorts but were not statistically significant (Figure 3O). Nonclassical MØ/monocytes were not detected in the airways of most individuals (Figure 3P). With regards to innate immune lineages in the blood (Figure 4, I–P), the only distinction between CF-NTM^{POS} and CF-NTM^{NEG} cohorts pertained to NK cells. Namely, we observed decreased NK cell frequencies among our CF-NTM^{POS}

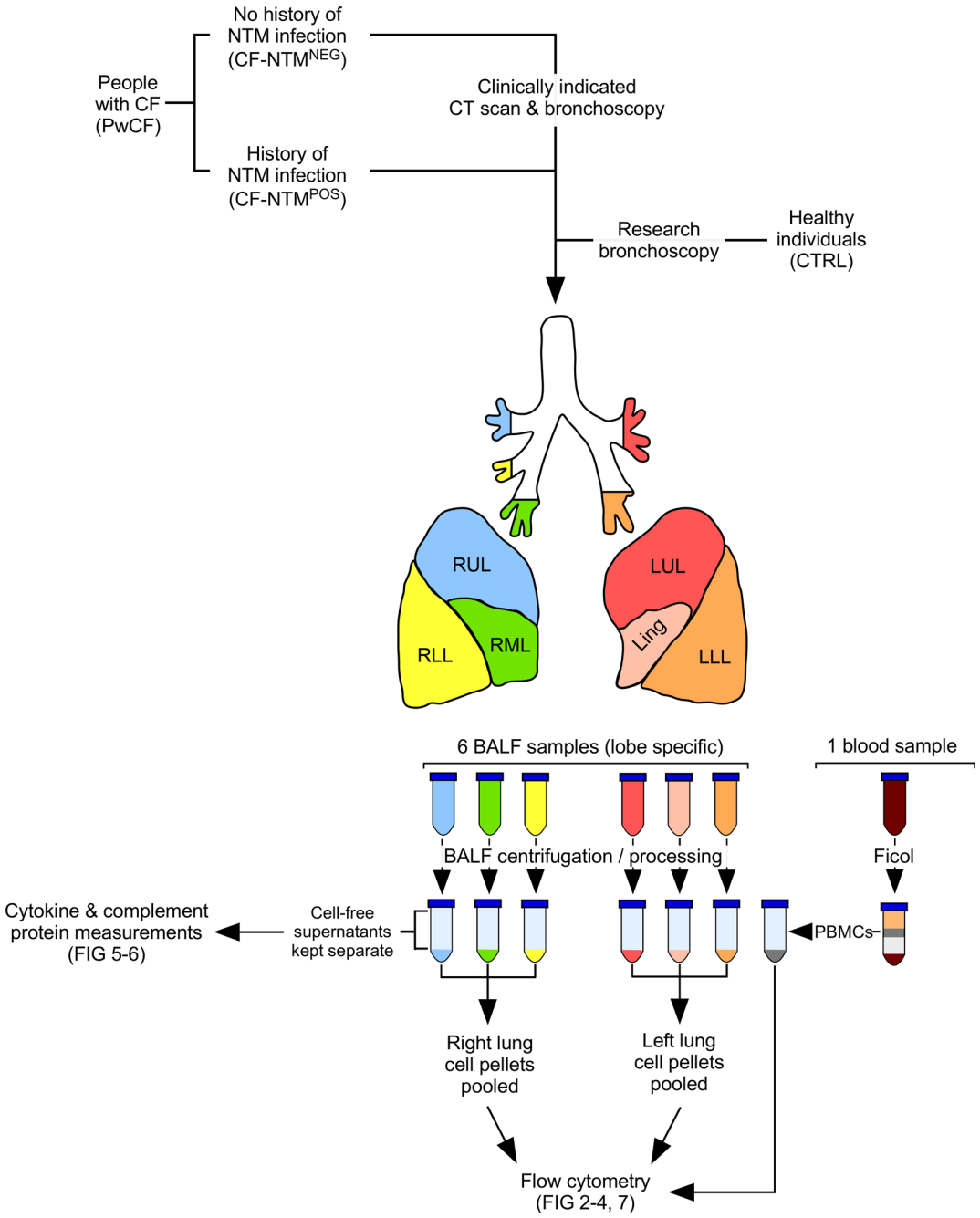

Figure 1. Overview of our study and experimental design. Adult individuals with CF and a history of being CF-NTM^{POS} and CF-NTM^{NEG} consented to our study after having scheduled a clinically indicated CT scan and bronchoscopy. CTRL individuals likewise consented to a research bronchoscopy. All bronchoscopies were done by the same individual (author DH). At the time of the bronchoscopy, blood- and lobe-specific BALF samples from the RUL, RML, RLL, LUL, Ling, and LLL were collected and kept separate. Once BALF samples were centrifuged and otherwise processed in a laboratory, cell-free supernatants from each lobe were collected and frozen for downstream cytokine measurements (the data from which are shown in Figures 5 and 6). To have a sufficient number of cells for flow cytometry, cell pellets from the right lung lobes (RUL, RML, and RLL) were pooled, as were the cell pellets from the left lung lobes (LUL, Ling, and LLL). The right lung BALF cells, left lung BALF cells, and PBMCs of each individual were immediately used for phenotypic and functional flow cytometry analysis (the data from which are shown in Figures 2–4, and 7).

cohort relative to CF-NTM^{NEG} (Figure 4I), which mirrored the airway NK cell level differences between these 2 cohorts (Figure 3I). It was noted that the CF-NTM^{NEG} cohort had a higher frequency of circulating ILC1 cells relative to CTRL whereas the CF-NTM^{POS} cohort did not (Figure 4J), and that the CF-NTM^{POS} cohort had generally (albeit insignificantly) higher frequencies of circulating classical MØ/monocytes (Figure 4N) and circulating intermediate MØ/monocytes (Figure 4O).

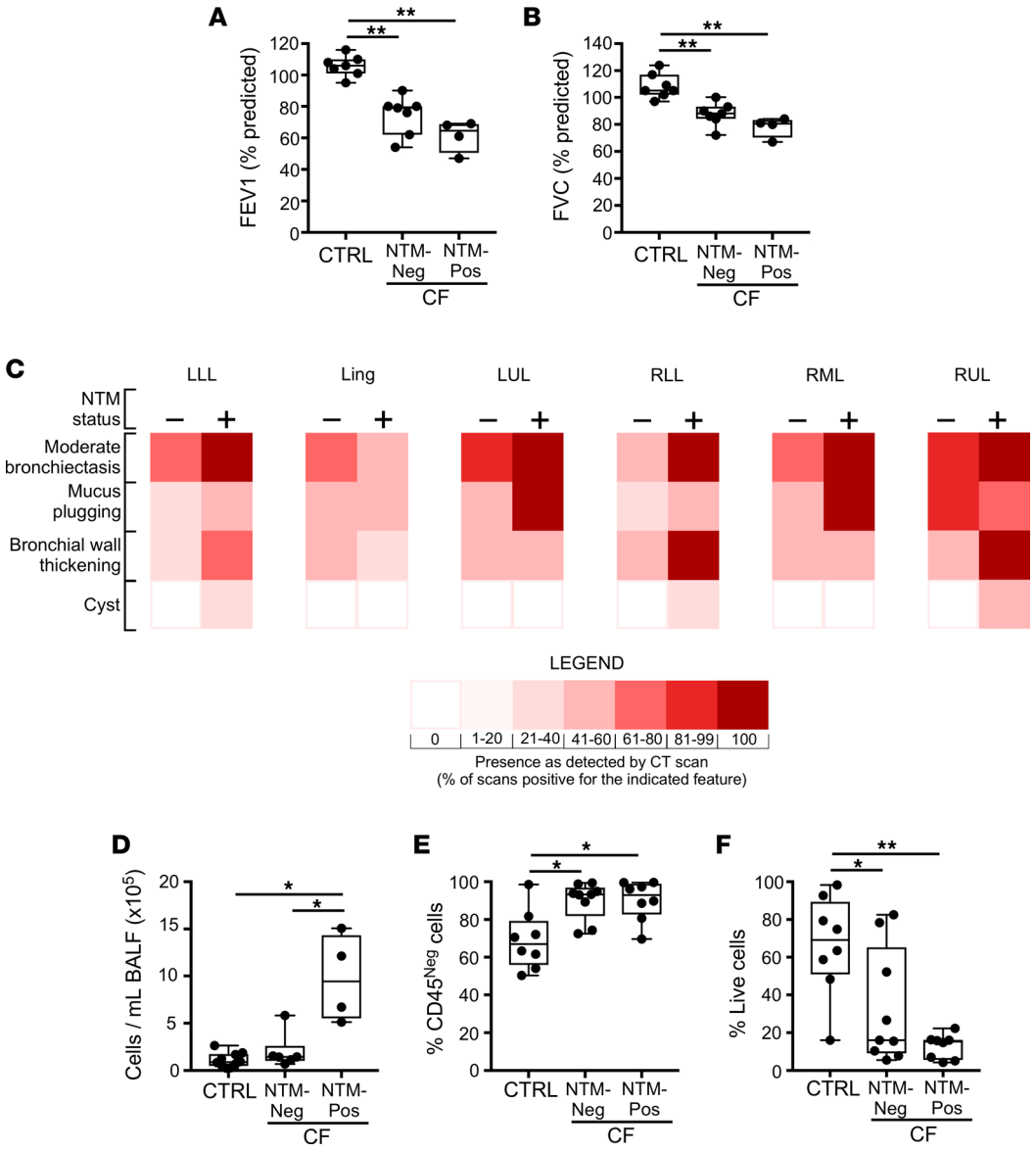

Figure 2. CF-NTM^{POS} lungs exhibit more tissue damage that is concentrated in the right and upper lobes. (**A** and **B**) FEV_1 and FVC were measured prior to bronchoscopy for each individual in our CTRL, CF-NTM^{NEG}, and CF-NTM^{POS} cohorts. Shown are the mean percentage predicted FEV_1 in A and the mean percentage predicted FVC values in B for each cohort. (**C**) CT scan findings for each lobe (LLL, Ling, LUL, RLL, RML, and RUL) based on an individual's NTM cohort status (- or +). Colors represent the percent of individuals in that cohort who had the following features in the specified lobe: moderate bronchiectasis, mucus plugging, bronchial wall thickening, and 1 or more cysts. (**D**–**F**) BALF from the same individuals was collected and used to prepare noncellular and cellular fractions (see Supplemental Figure 1), the latter of which were counted and stained with a viability dye and CD45-specific Ab. Shown are the total BALF cell counts in D and the CD45 frequency in E of each cohort, as well as the proportion of live BALF cells in each cohort in F. Bars represent mean ± SD; *P = 0.05, **P = 0.005 as determined by 1-way ANOVA.

CF-NTM^{POS} airways are distinguished by a hyperinflammatory cytokine profile

In addition to immune cells, cytokines and other soluble factors (e.g., complement) also influence the progression of lung pathology. To identify soluble factors that distinguish CF-NTM^{NEG} and CF-NTM-^{POS} airways from one another, we used a multiplex approach to measure the concentrations of multiple cytokines and complement proteins in BALF of each lung lobe (RUL, RML, RLL, LUL, Ling, and LLL). Cytokines that distinguished CF-NTM^{POS} and CF-NTM^{NEG} airways from one another and their associated modular analyses are shown in Figure 5 (heatmap format) and Supplemental Figure 3 (dot plot format), with modular designations being based on common immune origins or effects. Cytokines

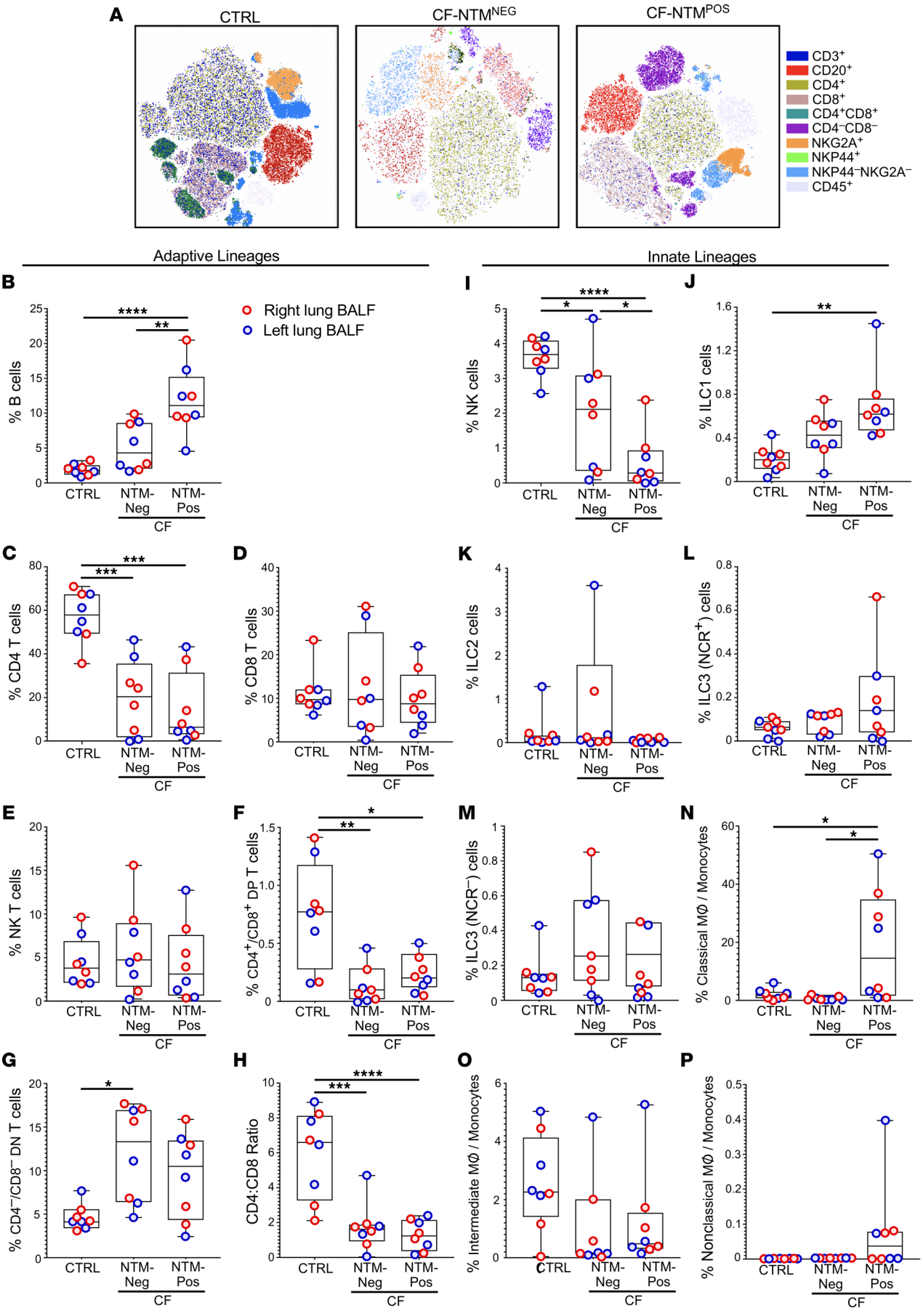
A
CTRL
CF-NTM^NEG
CF-NTM^POS
CD3+
CD20+
CD4+
CD8+
CD4+CD8+
CD4−CD8−
NKG2A+
NKP44+
NKP44−NKG2A−
CD45+
Adaptive Lineages
Innate Lineages
Right lung BALF
Left lung BALF
B
% B cells
C
% CD4 T cells
D
% CD8 T cells
E
% NK T cells
F
% CD4+/CD8+ DP T cells
G
% CD4−/CD8− DN T cells
H
CD4:CD8 Ratio
I
% NK cells
J
% ILC1 cells
K
% ILC2 cells
L
% ILC3 (NCR+) cells
M
% ILC3 (NCR−) cells
N
% Classical MØ / Monocytes
O
% Intermediate MØ / Monocytes
P
% Nonclassical MØ / Monocytes
CTRL
NTM-Neg
NTM-Pos
CF

Figure 3. CF-NTM^{POS} airways are distinguished by changes in multiple innate and adaptive immune lineage frequencies. BALF cells from individuals in our 3 cohorts (CTRL, CF-NTM^{NEG}, and CF-NTM^{POS}) were used for multidimensional flow cytometry analysis. (**A**) t-SNE analysis of the cumulative flow cytometry data from each cohort, wherein each cluster neighborhood represents a unique immune subset. Using the gating scheme shown in Supplemental Figure 2, we measured the frequencies of (**B**) B cells, (**C**) CD4 T cells, (**D**) CD8 T cells, (**E**) NKT cells, (**F**) CD4$^+$CD8$^+$ DP T cells, (**G**) CD4$^-$CD8$^-$ DN T cells, (**H**) CD4:CD8 T cell ratio, (**I**) NK cells, (**J**) ILC1 cells, (**K**) ILC2 cells, (**L**) ILC3 NCR$^+$ cells, (**M**) ILC3 NCR$^-$ cells, (**N**) classical MØ/monocytes, (**O**) intermediate MØ/monocytes, and (**P**) nonclassical MØ/monocytes. To observe general trends across cohorts, the data from right and left lung BALF are combined to generate each box and whisker plot; individual data points are, however, colored red or blue to indicate whether the data point originated from a right or left lung BALF, respectively. Asterisks indicate those group differences that were statistically significant as determined by 1-way ANOVA (*$P < 0.05$; **$P < 0.005$; ***$P < 0.0005$; ****$P < 0.0001$).

and complement proteins that distinguished CTRL airways from those of PwCF regardless of NTM infection history are shown in Figure 6 and Supplemental Figure 4. The patterns that emerged from our descriptive analysis of these data are as follows.

CF-NTM^{POS} airways have high concentrations of cytokines that promote B cell growth, MØ/monocyte attraction, T_H1/T_H17 polarization, granulocyte attraction, and epithelial damage. Consistent with their having elevated frequencies of B cells (Figure 3B) and MØs (Figure 3N), CF-NTM^{POS} airways had the highest concentrations of soluble CD40L (sCD40L), IL-10, IL-5, and BCA-1, each of which promotes B cell proliferation or chemoattraction), as well as high concentrations of M-CSF, Fractalkine, MIP1β, MCP-4, I-309, MCP-2, and MIP1Δ (each of which promotes MØ/monocyte development or chemoattraction) (Figure 5A). CF-NTM^{POS} airways also had higher concentrations of cytokines associated with T_H1/T_H17 polarization and responsiveness (IFN, IL-17A, IL-17E/IL-25, IL-17F, IL-23, IL-1β, IL-1α, IL-9, TGFα, and IL-21), granulocyte maturation and chemoattraction (IL-8, Eotaxin-3, Eotaxin, ENA78, and G-CSF), and epithelial damage or damage response (EGF, FGF2, TRAIL, IL-1RA, and PDGF-AA). Other cytokines that were more concentrated in CF-NTM^{POS} airways (relative to CF-NTM^{NEG}) included those that promote T cell chemoattraction or development (6CKine, CTACK, SDF-1a+B, IL-28A, and IL-15, dendritic cell maturation (thymic stromal lymphopoietin [TSLP], FMS-like tyrosine kinase 3 ligand [FLT-3L]), mucin secretion (IL-13, IL-33, and IL-1β; ref. 28) and the hematopoietic factors stem cell factor (SCF) and thrombopoietin (TPO). The only cytokines less concentrated in CF-NTM^{POS} airways compared with CF-NTM^{NEG} airways were GM-CSF and MCP-1 (Figure 5B).

Complement pathway members are largely absent from the airways of PwCF, regardless of NTM infection history. Complement is an important contributor to clearance of microorganisms and damaged cells. Surprisingly, nearly all members of the complement cascade were lower in CF-NTM^{NEG} and CF-NTM^{POS} airways, relative to CTRL, including complement factors C3, B, 1a, H, C1q, and C5a (Figure 6A). The only exceptions to this were complement factors C4 and D, which notably were only present in CF-NTM^{POS} airways. Additional cytokines that were less concentrated in PwCF airways (regardless of NTM infection history) relative to CTRL included IL-6, IP10, VEGFa, Eotaxin-2, GROα, MIG/CXCL9, RANTES, IL-18, MDC, and TARC (Figure 6A). Only 3 cytokines (IL-20, IL-16, and TNFβ) were equally concentrated in CF and CTRL airways (Figure 6B). The cytokines that were elevated in the airways of PwCF include those that influence T cells (IL-12p40, IL-12p70, IL-27, IL-2, IL-22, and IL-4) or are otherwise involved in antiviral responses, epithelial/mesenchymal differentiation, and chemoattraction (IFNα2, PDGF-AB/BB, LIF, MCP-3, IL-3, and MIP1α) (Figure 6C).

High levels of IFNγ and IL-17 in CF-NTM^{POS} airways do not reflect systemic differences in T_H or ILC polarization

Having observed high levels of IFNγ and IL-17 cytokines in the BALF of CF-NTM^{POS} airways (Figure 5A), we performed intracellular cytokine staining on stimulated PBMCs from the same individuals to determine if T cells from individuals who are CF-NTM^{POS} have a greater capacity for IFNγ or IL-17 production. Since innate lymphocytes are also capable of producing IFNγ and IL-17, we also stained and examined levels of these cytokines in NK cells, ILC1, and ILC3 (NCR$^-$) cells. ILC2 and ILC3 (NCR$^+$) cells were excluded from analysis because their frequencies among PBMCs were too low to draw meaningful conclusions (Figure 4, K and L). These data indicate that although circulating CD4 T cells from individuals who are CF-NTM^{POS} tended to produce more IFNγ (Figure 7A) and IL-17 (Figure 7B), these trends were not statistically significant. The frequencies of cytokine-producing NK, ILC1, and ILC3 (NCR$^-$) cells were also similar across CTRL, CF-NTM^{NEG}, and CF-NTM^{POS} cohorts. These intracellular cytokine data suggest that elevated levels of IFNγ and IL-17 in the CF-NTM^{POS} airways (Figure 5A) are a local response to the lung environment and do not represent a systemic increase in T cell or ILC capacity to produce these cytokines.

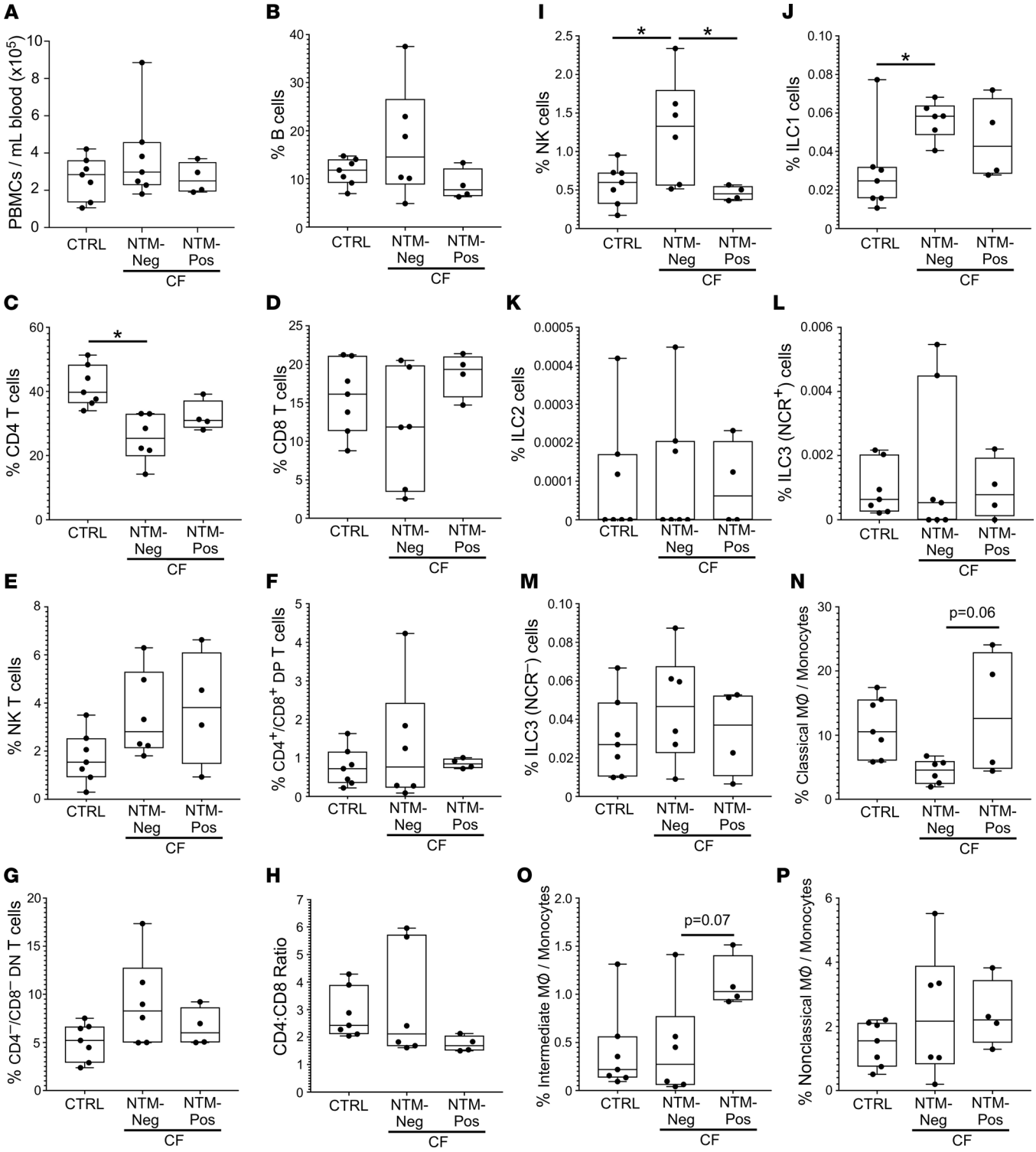

Figure 4. Circulating immune lineage frequencies are largely similar between individuals who are CF-NTM^{POS} and CF-NTM^{NEG}. Blood from individuals in each cohort was collected at the time of bronchoscopy and used to determine circulating immune subset frequencies, using the same flow cytometry panel and gating strategy as that used to determine airway immune subset frequencies. Shown for each cohort are (**A**) PBMC concentrations and frequencies of circulating (**B**) B cells, (**C**) CD4 T cells, (**D**) CD8 T cells, (**E**) NKT cells, (**F**) $CD4^+CD8^+$ DP T cells, and (**G**) $CD4^-CD8^-$ DN T cells, as well as (**H**) the ratio of CD4:CD8 T cells in the blood of each cohort. Likewise, shown are the frequencies of circulating (**I**) NK cells, (**J**) ILC1 cells, (**K**) ILC2 cells, (**L**) ILC3 (NCR^+) cells, (**M**) ILC3 (NCR^-) cells, (**N**) classical MØ/monocytes, (**O**) intermediate MØ/monocytes, and (**P**) nonclassical MØ/monocytes. Closed circles represent individual donor data; box and whiskers, means with error bars at the minimum and maximum (*$P < 0.05$ by 1-way ANOVA).

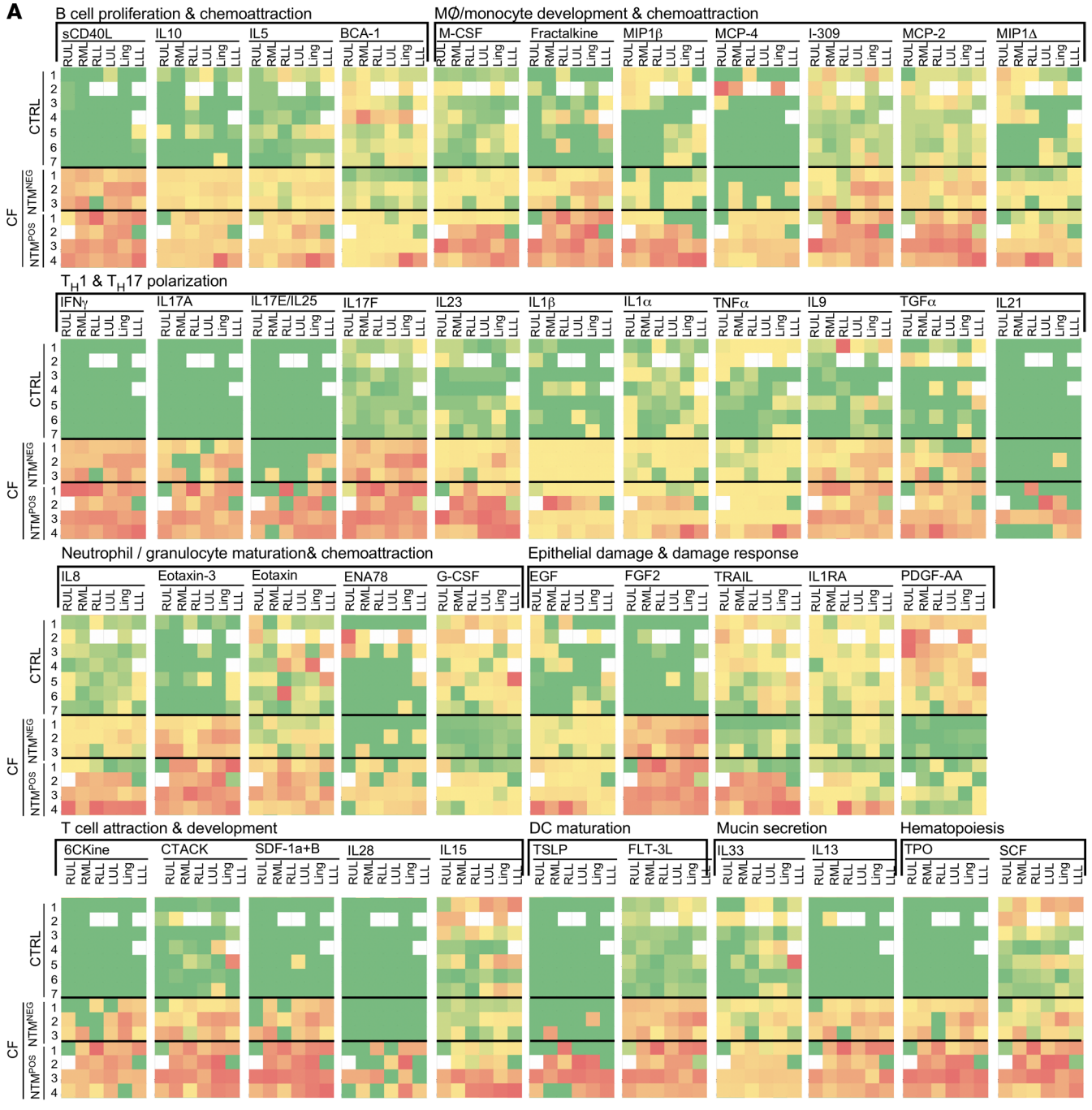

Figure 5. CF-NTM^{POS} airways have high concentrations of cytokines that promote B cell growth, MØ/monocyte attraction, T_H1/T_H17 polarization, granulocyte attraction, and epithelial damage. BALF samples from each lung lobe (RUL, RML, RLL, LUL, Ling, and LLL) were collected from individuals in each cohort and processed into cellular and noncellular fractions, the latter of which were used to measure the protein concentrations of multiple cytokines. Shown in heatmap format are those cytokines that distinguished CF-NTM^{POS} airways from CF-NTM^{NEG} airways as determined by statistical analyses (Supplemental Figure 3), including (**A**) BALF cytokines that were higher in CF-NTM^{POS} airways relative to CF-NTM^{NEG} airways, as well as (**B**) BALF cytokines that were lower in CF-NTM^{POS} airways relative to CF-NTM^{NEG} airways. For each heatmap, rows represent data from a specified individual and columns represent data from the specified lung lobe. Since the concentration range for each cytokine is different, green and red represent the lower and higher values of a given concentration range, respectively, relative to the mean (yellow). White boxes represent samples for which there was an insufficient amount of material for cytokine measurement. Specific values for these same cytokine and sample data are shown in Supplemental Figure 3.

Immune correlates of NTM infection history status are primarily observed in the lung and exhibit interlobar variability

To identify immune correlates of CF or NTM infection history status, we performed a principal components analysis (PCA) incorporating the blood and airway immune lineage frequency values of each individual in our CTRL, CF-NTM^{NEG}, and CF-NTM^{POS} cohorts (Figure 8), as well as their corresponding lobe-specific cytokine levels (Figure 9). We stratified the PCA of immune cell frequencies by tissue (blood and left and right lung segments) because we observed differing degrees of correlation based on the tissue examined (Figure 8A). The PCA of cytokine concentrations was, likewise, stratified by lobe due to differing degrees of correlation based on the lobe examined (Supplemental Figure 5).

At least 3 principal components (PCs) were sufficient to explain variation in our immune cell frequencies and cytokine concentration assessments (Supplemental Figure 6 and Supplemental Tables 2 and 3) With regards to the PCA of immune cell frequencies (Figure 8), among CTRL individuals, we observed tight clustering of PC1 and PC2 scores in the blood (Figure 8B, blue), left lung (Figure 8C, blue) and — to a lesser extent — the right lung (Figure 8D, blue). There was separation between CTRL and CF cohorts with respect to PC1 and PC2 scores in blood and left lung segment, where CF-NTM^{NEG} and CF-NTM^{POS} cohorts were largely overlapping (Figure 8C, red and green) with PC1 scores. Optimal separation between CF-NTM^{NEG} and CF-NTM^{POS} cohorts, however, was achieved in the right lung segment (Figure 8D, red and green), with higher PC1 scores representing variables uniquely driven by NTM status, the highest positive loadings being B cells, classical MØ, and ILC1 cells (Supplemental Table 2). With regards to the PCA of lobe-specific cytokine concentrations, clear separation was observed between individuals in our CTRL cohort (Figure 9, A–F, blue data points) and 2 CF cohorts (Figure 9, A–F, red and green data points) in each of the 6 lung lobes (LUL, Ling, LLL, RUL, RML, and RLL) (Figure 9, A–C, E, and F). Among PwCF, the CF-NTM^{NEG} and CF-NTM^{POS} cohorts separated from one another with respect to the PC2 scores, which were generally higher among individuals who are CF-NTM^{POS}, the most common and highest positive loadings being cytokines associated with BCA-1, MØ/monocyte attraction (MIP1β, MIP1Δ), epithelial/endothelial damage (TRAIL, PDGF-AA), neutrophil attraction and activation (ENA78, IL-8), granulocyte maturation (GCSF), T cell proliferation (IL-15), and complement components C4, C5a, and Factor D (Supplemental Table 3). Optimal separation between CF-NTM^{NEG} and CF-NTM^{POS} cohorts was observed in the RUL (Figure 9D), which is a lobe most affected by tissue damage (Figure 2C). Collectively, these PCA indicate that immune correlates of NTM infection history status include differences in lineage frequencies and cytokine concentrations, with differences being most pronounced in the right and upper lobes.

Discussion

All PwCF encounter unique immunological challenges throughout life. Since those with a history of NTM infection are more likely to experience severe forms of lung disease and complications over the course of CF treatment, including allograft rejection following lung transplant, we performed the above study to determine if the CF-NTM^{POS} lung immune environment is distinct from CF-NTM^{NEG} lungs or contains targets for HDTs, which may improve antimycobacterial therapy outcomes. Although many differences were noted among PwCF based on their NTM infection history, as well as between PwCF and healthy controls, the 4 most notable observations and their potential clinical significance are as follows.

The most unexpected observation was that CF-NTM^{POS} airways contained higher frequencies of B cells relative to CF-NTM^{NEG} airways. Although B cells' contribution to the most common form of mycobacterial disease (TB) has long been a topic of controversy, in the context of NTM infection, there are clinical studies that support B cells having a pathogenic role, including the positive correlation between pulmonary NTM infection status and circulating IgG levels (29, 30) and their suppression of anti-mycobacterial immune responses via autoantibodies that neutralize cytokines (31, 32) or weaken epithelial integrity (33). The increased B cell frequencies and associated cytokines (sCD40L, IL-10, IL-5, and BCA1) observed in CF-NTM^{POS} airways is also noteworthy because these individuals are more likely to die or experience morbidity following removal of their CF lung and replacement with a healthy allogeneic lung (34–37). There are multiple reasons for lung allograft failure in the setting of CF, including overall pretransplant health and postoperative airway dehiscence; however, should B cells of individuals who are CF-NTM^{POS} have an inherently better ability to migrate into the lung or expand, the Abs produced by these cells may potentially accelerate the allograft response and transplant rejection.

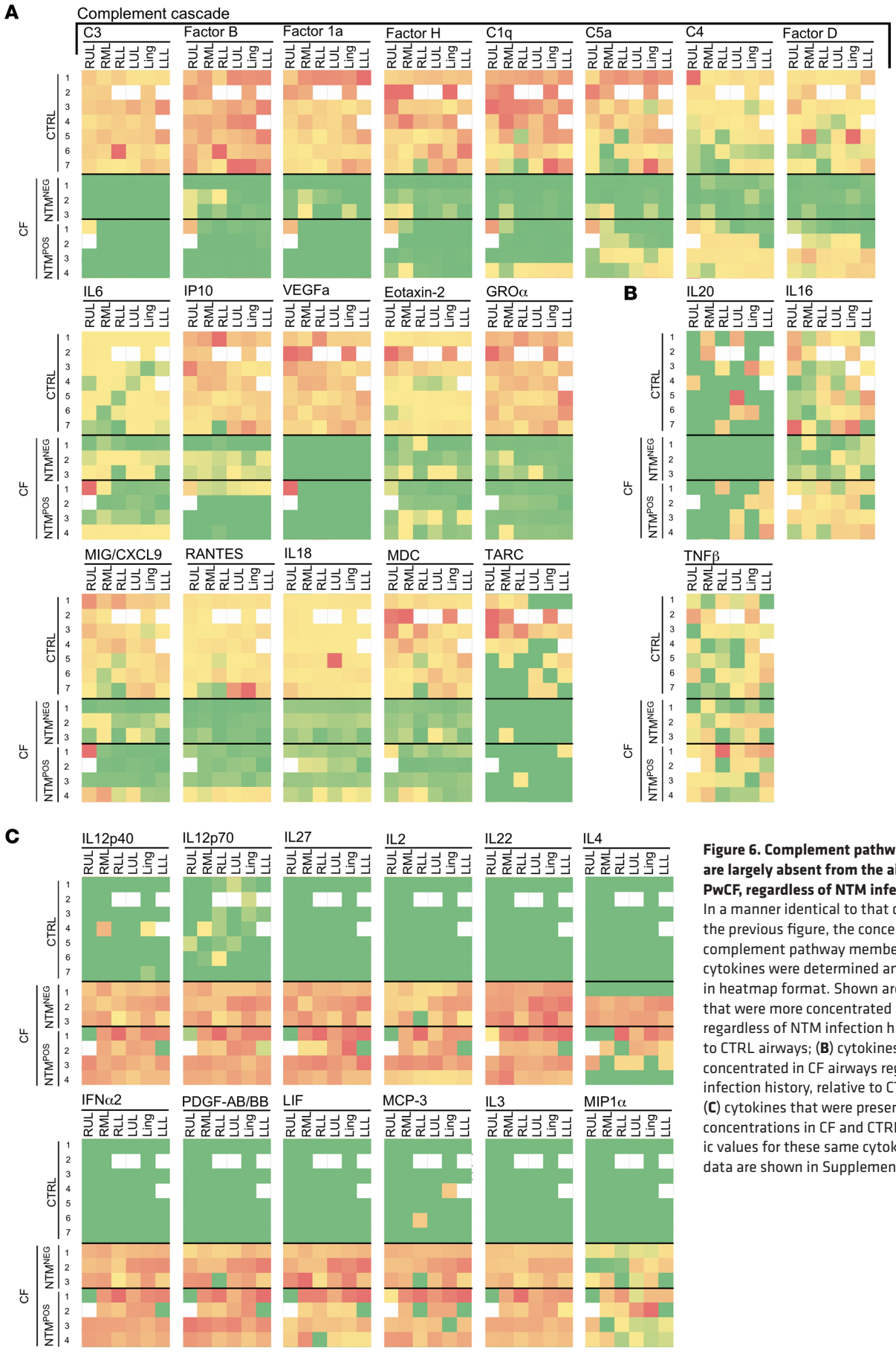

Figure 6. Complement pathway members are largely absent from the airways of PwCF, regardless of NTM infection history. In a manner identical to that described in the previous figure, the concentrations of complement pathway members and multiple cytokines were determined and represented in heatmap format. Shown are (**A**) cytokines that were more concentrated in CF airways regardless of NTM infection history, relative to CTRL airways; (**B**) cytokines that were less concentrated in CF airways regardless of NTM infection history, relative to CTRL airways; and (**C**) cytokines that were present at equivalent concentrations in CF and CTRL airways. Specific values for these same cytokine and sample data are shown in Supplemental Figure 4.

A second noteworthy feature of the CF-NTM^{POS} airway were the high and low frequencies, respectively, of MØ/monocytes and NK cells relative to CF-NTM^{NEG} airways. Replication within MØ/monocytes is a pathogenesis mechanism for many *Mycobacteria* species. Since CF MØ/monocytes also have impaired antimicrobial activity (38–40), their abundance in the CF-NTM^{POS} airway along with cytokines that support their development and attraction (M-CSF, Fractalkine, MIP1β, MCP4, I309, MCP-2, and MIP1Δ) may represent an ideal environment for NTM replication. Although NK cells lack direct bactericidal capacity, their absence from the airways may indirectly contribute to NTM infection since NK cells clear the lungs of influenza, cytomegalovirus (CMV), and other viruses that may predispose the lung to secondary mycobacterial infections (41, 42). The low NK cell frequencies we observed potentially stem from altered NK cell development (as opposed to NK cell death), as the proportion of ILC1 cells (a lineage to which NK cell can convert; ref. 43) is correspondingly higher in CF-NTM^{POS} airways, as is the concentration of a cytokine that promotes NK-to-ILC conversion (i.e., IL-15; ref. 44). Evidence of altered T cell development was also noted in both CF cohorts (i.e., airway frequencies of DP and DN T cells differed from CTRL individuals), supporting the concept of *CFTR* being a regulator of T lymphopoiesis and thymic homing (45).

Third, there was remarkable concordance between the location of lung tissue damage (as determined by CT) and the biogeographical distribution of inflammatory markers in CF-NTM^{POS} airways (as determined by PCA of our collected data). Healthy CTRL lungs comprise biogeographical regions that vary in blood gas tension, blood perfusion, pH, temperature, and microbiological factors (46, 47). Until now the relationship between CF, NTM infection, and lung immune biogeography was unknown. Compared to our CF-NTM^{NEG} cohort, the lungs of our CF-NTM^{POS} cohort exhibited more tissue damage that was concentrated in right and upper lobes. Likewise, the same CF-NTM^{POS} lungs were distinct in terms of their right and upper airway immune profiles, including high concentrations of cytokines that damage epithelial barriers and drive T_H17 polarization, granulocyte chemoattraction, and mucin secretion. TRAIL, one of the cytokines that most distinguished CF-NTM^{POS} from CF-NTM^{NEG} airways, damages epithelial barriers via induction of epithelial cell apoptosis and necrosis (48). T_H17-associated cytokines cause fibrosis by promoting epithelial to mesenchymal transition, myofibroblast differentiation, and extracellular matrix production. High levels of T_H17 cytokines are consistent with other models of mycobacteria-induced immunopathology (TB); however, in the case of our CF-NTM^{POS} cohort, this was not accompanied by elevated frequencies of airway T_H cells. Low frequencies of airway T_H cells belie their inflammatory nature, however, as *CFTR*-deficient T cells are hyperresponsive to TCR activation (49). IL-17 also causes epithelial cells to express mucin proteins (50) and secrete neutrophil chemoattractants that were also elevated in the CF-NTM^{POS} airways (e.g., G-CSF, IL-8). Neutrophil degranulation causes the release of multiple proteases that do not discriminate between pathogens versus host, leading to further breakdown of epithelial integrity.

Fourth and finally, the concentrations of nearly all complement pathway members were low in the airways of PwCF, regardless of NTM infection history. The complement pathway is an innate effector mechanism that helps kill and clear a variety of microbes, including viruses, bacteria, and fungi. Bronchial epithelial cells from PwCF are certainly capable of secreting a number of complement proteins, albeit some at levels significantly lower than those of non-CF bronchial epithelial cells (51). It has also been demonstrated that CF airway C5a levels are highest in those with more inflamed lungs (52, 53) (which is consistent with our observation of C5a being higher in CF-NTM^{POS} versus CF-NTM^{NEG} airways). Still, the highest complement concentrations in CF-NTM^{POS} BALF is far below the average complement concentrations of CTRL BALF. We are not the first to observe this, as an unbiased proteomics approach also identified a complement module comprising several complement proteins (C1QA, C1QB, C1QG, C2, C4b, C5, C6, and Clusterin) as being depleted from BALF of PwCF (54), and many of these proteins were decreased in the lungs of *CFTR* knockout ferrets (55). Although early studies ruled out genetic complement deficiency as a contributing cause of CF (56, 57), our study and those referenced above suggest low complement levels may be an overlooked explanation of why PwCF are predisposed to opportunistic viral, bacterial, and fungal infections.

We recognize the limitations of our study, which are its modest size, being cross-sectional (as opposed to longitudinal) and our not knowing the *CFTR* genotype of healthy controls. Our study was completed before the rollout of newer CFTR modulators, which have improved the lung function and quality of life for many PwCF. It is not yet known what impact this important new drug combination will have on infections caused by NTM. On the one hand, *CFTR* modulation is likely to ease the immunological challenges on the CF lung, since increased mucociliary clearance will presumably shorten the exposure of airways to newly inhaled particulates and microbes; on the other hand, *CFTR*

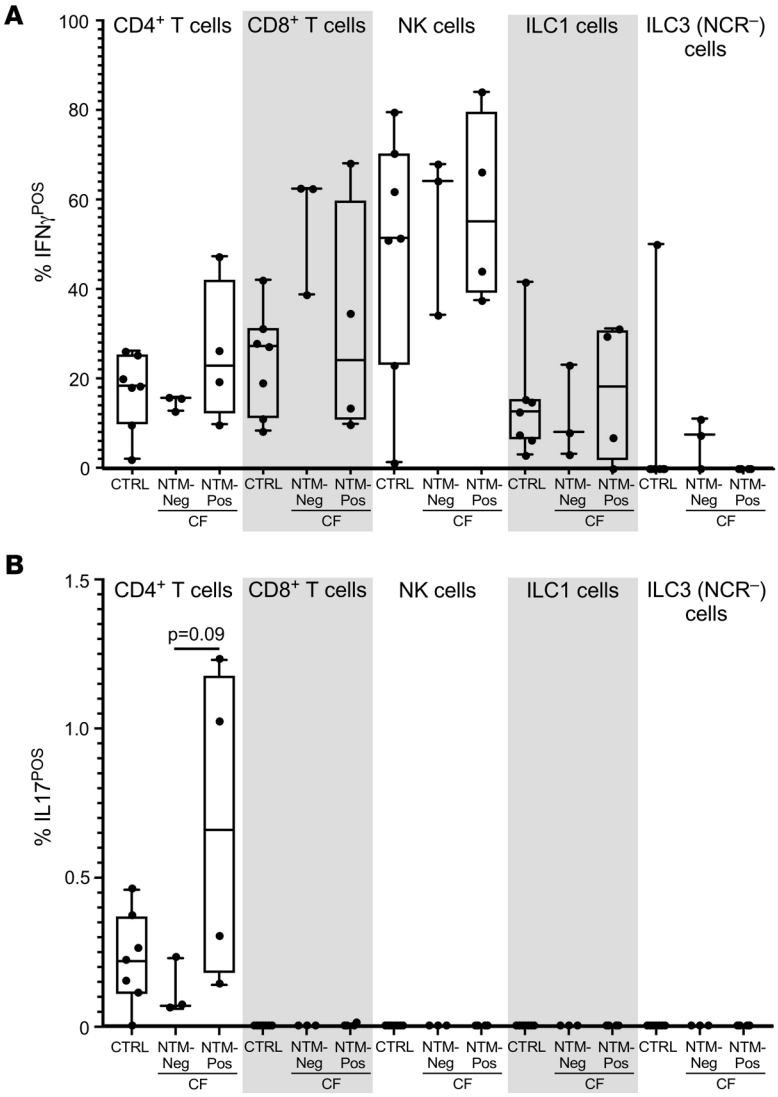

Figure 7. Circulating lymphocytes from individuals who are CF-NTM^{NEG} and CTRL-NTM^{POS} have similar IFNγ- and IL-17–producing capacity. PBMCs from individuals in each study cohort (CTRL, CF-NTM^{NEG}, and CTRL-NTM^{POS}) were stimulated in vitro and stained to identify 5 lymphocyte subsets (CD4$^+$ T cells, CD8$^+$ T cells, NK cells, ILC1, and ILC3) and quantify their production of IFNγ and IL-17. For each cohort and lymphocyte subset, the percentage of cells positive for (**A**) IFNγ or (**B**) IL-17 are shown. In each case, closed dots represent data from a given individual in the indicated cohort, with box and whiskers representing data from the entire cohort; significance was determined by 1-way ANOVA.

modulation may not be as effective in portions of the lung where damage has already occurred or where opportunistic pathogens have already established a niche (58). In spite of these limitations, we anticipate these data will be useful for guiding the development of HDTs to suppress lung inflammation or improve antibiotic efficacy in individuals who are CF-NTM^{POS}, and to inform future studies seeking to link immune biogeography to lung disease outcomes in individuals who are CF-NTM^{NEG} and CF-NTM^{POS} alike.

Methods

Patients and sample collection. Two PwCF cohorts were established for prospective BALF and blood collection: CF-NTM^{NEG} and PwCF with no history of mycobacteria positivity as determined by clinical assessment before or at the time of bronchoscopy; and CF-NTM^{POS} and PwCF with a history of mycobacteria positivity as determined by clinical assessment before or at the time of bronchoscopy. A CTRL cohort was also established, comprising local, age-matched, healthy individuals without CF. The demographic and physical

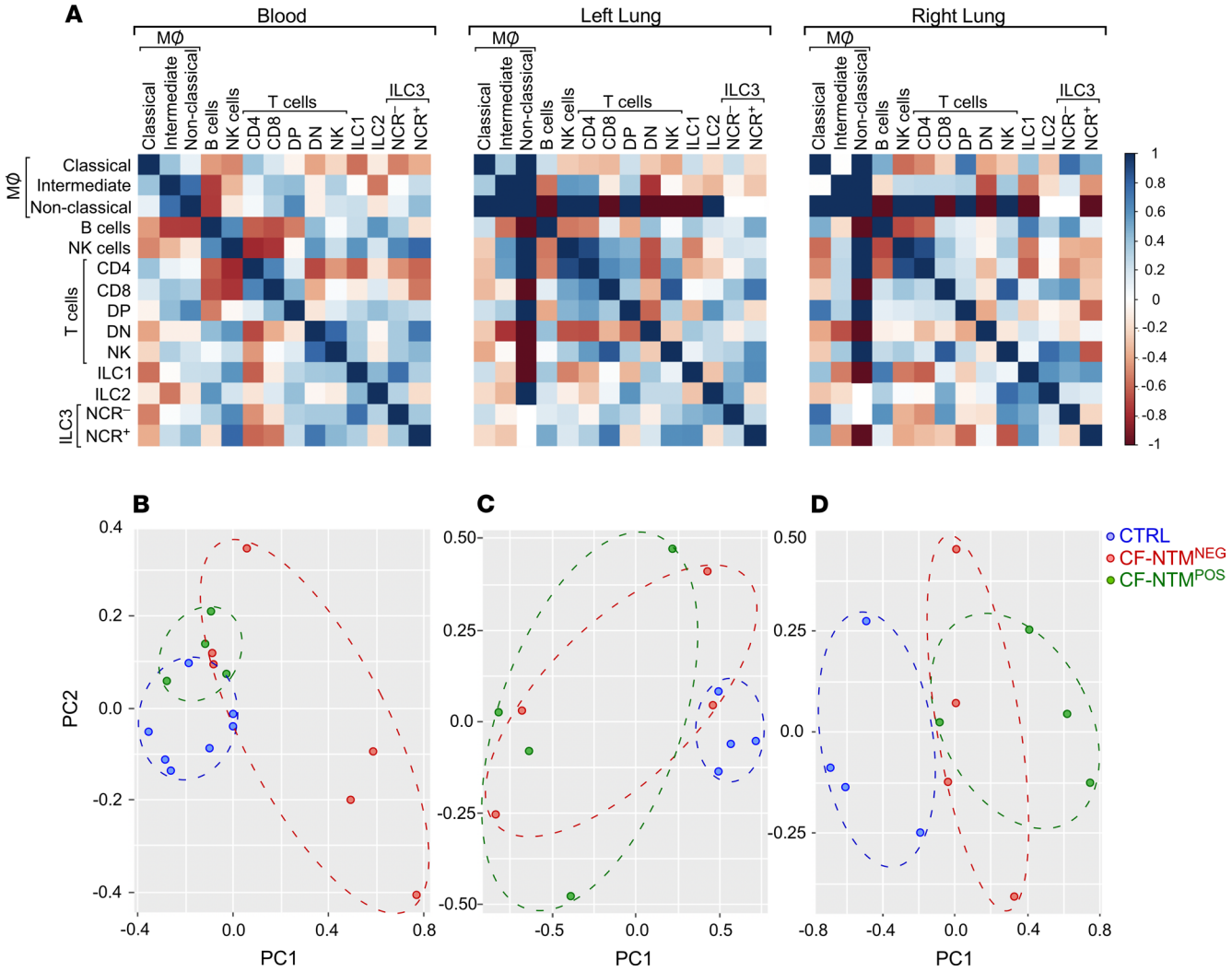

Figure 8. Cellular biomarker differences between individuals who are CF-NTM^{NEG} and CF-NTM^{POS} are pronounced in the right lung segment. Adaptive and innate immune subset frequency data from the blood, left lung, and right lung were analyzed via PCA to identify cellular correlates of CF status and NTM infection history status. (**A**) Correlation matrix of immune subset frequencies in blood, left lung, and right lung. (**B**–**D**) PC scores for the first and second components of immune cell frequencies from (**B**) blood, (**C**) left lung, and (**D**) right lung.

characteristics of each cohort are provided in Table 1, as are the *CFTR* genotypes represented in our PwCF cohorts. Lobe-specific CT scan and pulmonary function testing was performed prior to BALF collection. For both CF cohorts, BALF was collected during a clinically indicated bronchoscopy for functional endoscopic sinus surgery. BALF was collected from our CTRL cohort via a research bronchoscopy. A single individual (author DH) performed all bronchoscopies to limit variability in BALF collection technique. A total of 20 mL of sterile saline was instilled into each lobe of the right and left lung, with the Ling considered a separate lobe. Recovery of BALF was 40–50% of the total volume instilled, a portion of which was used for clinical microbiology testing per standards of care. Any NTM present were assigned a species designation based on a combination of growth profile characteristics (rapid versus slow growing), colony morphology, and MALDI-TOF per standards of care. The remaining BALF was placed on ice and transported to the research laboratory where flow cytometry was performed within an hour of sample collection.

BALF and blood processing. Each lobe-specific BALF sample was gently passed through sterile gauze to remove mucus and centrifuged (500 RCF, 6 min, 4°C) to separate the noncellular and cellular fractions. Following centrifugation, lobe-specific supernatant samples were kept separate (i.e., not pooled) for cytokine measurements. To have a sufficient number of cells for flow cytometry analysis it was necessary to pool the RUL, RML, and RLL cell fractions into a single sample representing all right lung BALF cells; LUL, Ling, and LLL cell fractions were likewise pooled into a single sample to represent all left lung

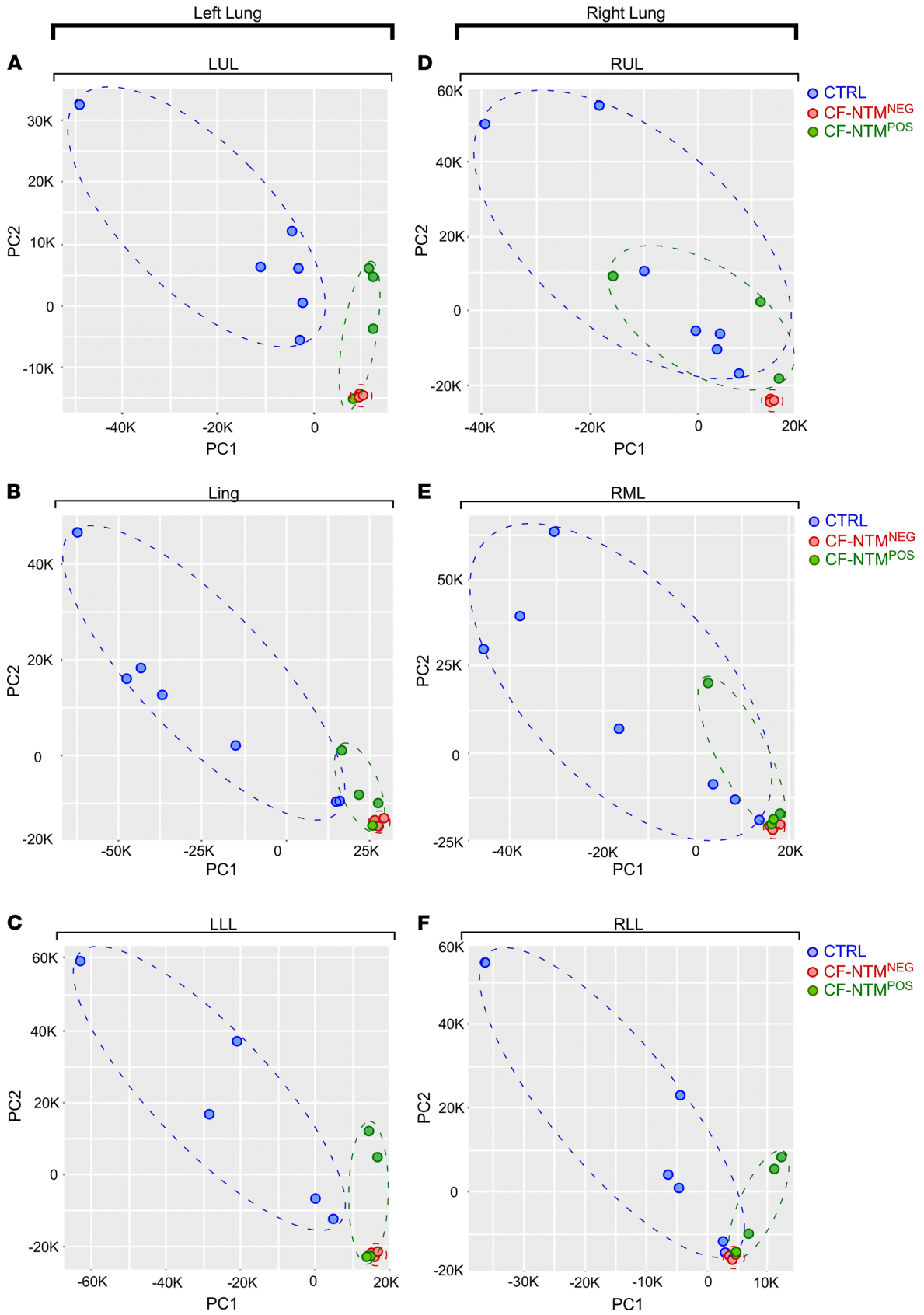

Figure 9. Cytokine and complement biomarker differences between individuals who are CF-NTM^{NEG} and CF-NTM^{POS} are pronounced in the RUL. Lobe-specific cytokine and complement concentration data from all individuals in each cohort were analyzed via PCA to identify correlates of CF status and NTM infection history status. PCA scores for the first and second components of cytokine concentrations from the left lung lobes (**A**) LUL, (**B**) Ling, and (**C**) LLL, as well as the right lung lobes (**D**) RUL, (**E**) RML, and (**F**) RLL.

BALF cells. Paired blood samples from the same individuals were centrifuged over a Ficoll gradient to PBMCs, which were subsequently counted and stained for immediate flow cytometric analysis of surface marker expression. Aliquots of PBMCs were also cryopreserved to enable intracellular cytokine staining at a later date, so PBMCs from all CTRL, CF-NTM^{POS}, and CF-NTM^{NEG} donors could be analyzed in the same manner at the same time.

Flow cytometry. All Abs used for flow cytometric analysis were purchased from commercial sources (BioLegend, Thermo Fisher, and Beckman Coulter). BALF cell and PBMC preparations were resuspended in ice-cold R10 media (RPMI 1640, 10% FBS, 2 mM L-glutamine, 100 U/mL penicillin G, and 100 μg/mL streptomycin), transferred into a 15 mL tube via a 100-μm filter and centrifuged (250 *g*, 7 min, 4°C). The cell pellet was again resuspended in R10 media, stained with a viability dye (LIVE/Dead Fixable Aqua, Invitrogen) per manufacturer instructions. It was then washed and mixed with a fluorescent Ab cocktail recognizing the following surface proteins (antibody clone, fluorescent conjugate are listed in parenthesis): CD45 (2D1, FITC); NKp44 (P44-8, PE-Cy7); CD161 (HP-3G10, Alexa Fluor 700); CD127 (A019D5, BV421); CD20 (2H7, BV605); CD117 (104D2, BV650); CD56 (HCD56, BV711); CD4 (SK-3, Super Bright 436); CD14 (TuK4, Pac Orange); CRTH-2 (301109, Alexa Fluor 647); CD8 (RPA-T8, Alexa Fluor 532); NKG2A (Z199, PE); CD16 (3G8, PE-Cy5); and CD3 (SP34-2, APC-Cy7). All Abs were previously titrated to determine the optimal concentration. For intracellular cytokine staining of cryopreserved PBMC preparations, PBMCs were thawed, transferred into prewarmed R10 media, and washed to remove residual cryopreservation media. PBMCs were then resuspended at 1–2′10^6 cells per mL in R10 and stimulated for 12 hours (37°C, 5% CO_2) with 50 ng/mL PMA (Sigma-Aldrich) and 1 μg/mL ionomycin (Sigma-Aldrich), in the presence of GolgiPlug (10 μg/mL; BD Biosciences). At the end of this stimulation period, cells were stained with a viability dye (LIVE/Dead Fixable Aqua, Invitrogen) and the surface Ab cocktail detailed above. After surface staining, cells were washed and fixed with 1x Intracellular Staining Permeabilization Wash Buffer (421002, BioLegend) and permeabilized with 1x Intracellular Staining Permeabilization Wash Buffer (421002, BioLegend) per the manufacturer protocols. Recommended amount of directly conjugated primary Abs for detection of intracellular antigens (IFNγ, TNF, and IL-17) were added. After washing and filtering cells through strainer capped FACS tubes, spectral flow cytometry data from stained cells were acquired on a Cytek Aurora instrument (Cytek Biosciences) and analyzed with FlowJo software (Tree Star). Prior to collecting spectral flow cytometry data on each sample, "fluorescence minus 1" controls (cells stained with all fluorochromes used in the experiment except 1) were performed for each marker prior to spectral unmixing.

Lobe-specific multiplex cytokine measurements. As detailed above, the noncellular fraction of BALF from each right lung lobe (RUL, RML, and RLL) and left lung lobe (LUL, Ling, and LLL) was collected from individuals in our CTRL, CF-NTM^{NEG}, and CF-NTM^{POS} cohorts. Aliquots were stored at −80°C and were shipped on dry ice to Eve Technologies, where the levels of multiple cytokines and other soluble factors were measured using the Millipore MILLIPLEX method (Human Complement P1 Featured 3-Plex Kit, HCMP1-03-03; Human Complement P2 Featured 5-Plex Kit, HCMP2-05-02; and Human Cytokine Array/Chemokine Array 71-403 Plex Panel, HD71).

PCA. We performed PCA separately of immune cell frequencies and cytokines using the "psych" package in R. We stratified each PCA result in immune cell frequencies to blood (overall) and left and right lung segments; results for cytokine data were stratified according to lobe section (RUL, RML, RLL, LUL, Ling, and LLL). Stratification was performed given that we observed differing degrees of correlation based on region in both immune cell (Figure 8A) and cytokine data (Supplemental Figure 5). Scree-plot and proportion-of-variance criteria were used to select the effective number of PCs. Scatterplots of scores for the first and second PCs were used to examine relationships of variables between and within experimental groups (CTRL, CF-NTM^{NEG}, and CF-NTM^{POS}). Factor loadings with magnitudes above 0.5 were considered influential for a given PC and assessed for overall structural pattern in each PCA.

Graphing and statistics. Graphs were prepared using Graph Pad Prism or Microsoft Excel, with the exception of dot plots and t-SNE dimensionality reduction plots (which were generated using FlowJo). Data were statistically analyzed using their bundled software. Statistical comparisons involving more than 2 experimental groups used ANOVA with followup column-to-column comparisons. All other statistical comparisons used Student's *t* test. Differences between groups were considered significant if $P < 0.05$ and are graphically indicated by 1 or more asterisks (*$P < 0.05$; **$P < 0.005$; ***$P < 0.0005$).

Study approval. This study was approved by the local Institutional Review Board with informed written consent obtained from all subjects prior to collection of research samples.

Author contributions

RKS performed experiments and acquired data, interpreted data, and revised the manuscript. YC, EG, MRM, and RDS interpreted data, performed statistical analysis, and revised the manuscript. AGZ, JCW, and LHS interpreted data and revised the manuscript. DH conceptualized and designed the study, collected samples for experiments for data acquisition, interpreted data, and drafted the initial manuscript. NPML and RTR conceptualized and designed the study, performed experiments, acquired data, interpreted data, and drafted the initial manuscript.

Acknowledgments

We would like to thank Holly Bookless and Kemba Days-Yancey of The Ohio State University (OSU) Clinical Research Center for their excellence and facilitating the research bronchoscopies associated with this study. This work was supported by funds from OSU and the Cystic Fibrosis Foundation (CFF), as administered by the Nationwide Children's Hospital (NCH) and OSU Cure Cystic Fibrosis Columbus (C3) Research Development Program, and by NIH grant R01AI121212 (to RTR).

Address correspondence to: Namal P. M. Liyanage, 788 Biomedical Research Tower (BRT), 460 W 12th Ave, Columbus, Ohio 43210, USA. Phone: 614.293.9114; Email: Namal.Liyanage@osumc.edu. Or to: Richard T. Robinson, 760 Biomedical Research Tower (BRT), 460 W 12th Ave, Columbus, Ohio 43210, USA. Phone: 614.293.4164; Email: Richard.Robinson@osumc.edu.

1. Shteinberg M, et al. Cystic fibrosis. *Lancet*. 2021;397(10290):2195–2211.
2. Elborn JS, et al. Report of the European Respiratory Society/European Cystic Fibrosis Society task force on the care of adults with cystic fibrosis. *Eur Respir J*. 2016;47(2):420–428.
3. Furukawa BS, Flume PA. Nontuberculous mycobacteria in cystic fibrosis. *Semin Respir Crit Care Med*. 2018;39(3):383–391.
4. Skolnik K, et al. Nontuberculous mycobacteria in cystic fibrosis. *Curr Treat Options Infect Dis*. 2016;8(4):259–274.
5. Qvist T, et al. Comparing the harmful effects of nontuberculous mycobacteria and Gram negative bacteria on lung function in patients with cystic fibrosis. *J Cyst Fibros*. 2016;15(3):380–385.
6. Floto RA, et al. US Cystic Fibrosis Foundation and European Cystic Fibrosis Society consensus recommendations for the management of non-tuberculous mycobacteria in individuals with cystic fibrosis: executive summary. *Thorax*. 2016;71(1):88–90.
7. Floto RA, et al. US Cystic Fibrosis Foundation and European Cystic Fibrosis Society consensus recommendations for the management of non-tuberculous mycobacteria in individuals with cystic fibrosis. *Thorax*. 2016;71 Suppl 1(suppl 1):i1–i22.
8. Qvist T, et al. Shifting paradigms of nontuberculous mycobacteria in cystic fibrosis. *Respir Res*. 2014;15:41.
9. Esther CR Jr., et al. Chronic Mycobacterium abscessus infection and lung function decline in cystic fibrosis. *J Cyst Fibros*. 2010;9(2):117–123.
10. Roux AL, et al. Multicenter study of prevalence of nontuberculous mycobacteria in patients with cystic fibrosis in france. *J Clin Microbiol*. 2009;47(12):4124–4128.
11. Martiniano SL, et al. Nontuberculous mycobacterial infections in cystic fibrosis. *Thorac Surg Clin*. 2019;29(1):95–108.
12. Bouso JM, et al. Household proximity to water and nontuberculous mycobacteria in children with cystic fibrosis. *Pediatr Pulmonol*. 2017;52(3):324–330.
13. Thomson RM, et al. Gastroesophageal reflux disease, acid suppression, and Mycobacterium avium complex pulmonary disease. *Chest*. 2007;131(4):1166–1172.
14. Saeed DK, et al. Mycobacterial contamination of bronchoscopes: challenges and possible solutions in low resource settings. *Int J Mycobacteriol*. 2016;5(4):408–411.
15. Hoiby N, et al. Diagnosis of biofilm infections in cystic fibrosis patients. *APMIS*. 2017;125(4):339–343.
16. Qvist T, et al. Chronic pulmonary disease with Mycobacterium abscessus complex is a biofilm infection. *Eur Respir J*. 2015;46(6):1823–1826.
17. Taylor JL, Palmer SM. Mycobacterium abscessus chest wall and pulmonary infection in a cystic fibrosis lung transplant recipient. *J Heart Lung Transplant*. 2006;25(8):985–988.
18. Zaidi S, et al. Mycobacterium abscessus in cystic fibrosis lung transplant recipients: report of 2 cases and risk for recurrence. *Transpl Infect Dis*. 2009;11(3):243–248.
19. Sanguinetti M, et al. Fatal pulmonary infection due to multidrug-resistant Mycobacterium abscessus in a patient with cystic fibrosis. *J Clin Microbiol*. 2001;39(2):816–819.
20. Ceron J, et al. Lung transplantation: Mycobacterium abscessus as a cause of graft dysfunction. *Breathe*. 2007;3(3):291–296.
21. Chernenko SM, et al. Mycobacterium abscessus infections in lung transplant recipients: the international experience. *J Heart Lung Transplant*. 2006;25(12):1447–1455.
22. Kilinc G, et al. Host-directed therapy to combat mycobacterial infections. *Immunol Rev*. 2021;301(1):62–83.
23. Scott JP, et al. Inhaled granulocyte-macrophage colony-stimulating factor for Mycobacterium abscessus in cystic fibrosis. *Eur Respir J*. 2018;51(4):1702127.
24. Hallstrand TS, et al. Inhaled IFN-gamma for persistent nontuberculous mycobacterial pulmonary disease due to functional IFN-gamma deficiency. *Eur Respir J*. 2004;24(3):367–370.
25. Chatte G, et al. Aerosolized interferon gamma for Mycobacterium avium-complex lung disease. *Am J Respir Crit Care Med*. 1995;152(3):1094–1096.

26. Milanes-Virelles MT, et al. Adjuvant interferon gamma in patients with pulmonary atypical Mycobacteriosis: a randomized, double-blind, placebo-controlled study. *BMC Infect Dis*. 2008;8:17.
27. Thomson RM, et al. Use of inhaled GM-CSF in treatment-refractory NTM infection. An open-label, exploratory clinical trial. *Eur Respir J*. 2021;58:OA1603.
28. Chen G, et al. IL-1β dominates the promucin secretory cytokine profile in cystic fibrosis. *J Clin Invest*. 2019;129(10):4433–4450.
29. Kim K, et al. Levels of anti-cytokine antibodies may be elevated in patients with pulmonary disease associated with non-tuberculous mycobacteria. *Cytokine*. 2014;66(2):160–163.
30. Amran FS, et al. Is pulmonary non-tuberculous Mycobacterial disease linked with a high burden of latent cytomegalovirus? *J Clin Immunol*. 2016;36(2):113–116.
31. Roerden M, et al. Simultaneous disseminated infections with intracellular pathogens: an intriguing case report of adult-onset immunodeficiency with anti-interferon-gamma autoantibodies. *BMC Infect Dis*. 2020;20(1):828.
32. Liu TT, et al. Nontuberculous mycobacterial infection with concurrent IgG4-related lymphadenopathy. *APMIS*. 2016;124(3):216–220.
33. Kato A, et al. B-lymphocyte lineage cells and the respiratory system. *J Allergy Clin Immunol*. 2013;131(4):933–957.
34. Friedman DZP, et al. Non-tuberculous mycobacteria in lung transplant recipients: prevalence, risk factors, and impact on survival and chronic lung allograft dysfunction. *Transpl Infect Dis*. 2020;22(2):e13229.
35. Hamad Y, et al. Outcomes in lung transplant recipients with Mycobacterium abscessus infection: a 15-year experience from a large tertiary care center. *Transplant Proc*. 2019;51(6):2035–2042.
36. Longworth SA, et al. Non-tuberculous mycobacterial infections after solid organ transplantation: a survival analysis. *Clin Microbiol Infect*. 2015;21(1):43–47.
37. Huang HC, et al. Non-tuberculous mycobacterium infection after lung transplantation is associated with increased mortality. *J Heart Lung Transplant*. 2011;30(7):790–798.
38. Robledo-Avila FH, et al. Dysregulated calcium homeostasis in cystic fibrosis neutrophils leads to deficient antimicrobial responses. *J Immunol*. 2018;201(7):2016–2027.
39. Tazi MF, et al. Elevated Mirc1/Mir17-92 cluster expression negatively regulates autophagy and CFTR (cystic fibrosis transmembrane conductance regulator) function in CF macrophages. *Autophagy*. 2016;12(11):2026–2037.
40. Assani K, et al. IFN-γ stimulates autophagy-mediated clearance of Burkholderia cenocepacia in human cystic fibrosis macrophages. *PLoS One*. 2014;9(5):e96681.
41. Walaza S, et al. Influenza and tuberculosis co-infection: a systematic review. *Influenza Other Respir Viruses*. 2020;14(1):77–91.
42. Cobelens F, et al. The convergent epidemiology of tuberculosis and human cytomegalovirus infection. *F1000Res*. 2018;7:280.
43. Bal SM, et al. Plasticity of innate lymphoid cell subsets. *Nat Rev Immunol*. 2020;20(9):552–565.
44. Hawke LG, et al. TGF-β and IL-15 synergize through MAPK pathways to drive the conversion of human NK cells to an innate lymphoid cell 1-like phenotype. *J Immunol*. 2020;204(12):3171–3181.
45. Lin Z, et al. CFTR regulates embryonic T lymphopoiesis via Wnt signaling in zebrafish. *Immunol Lett*. 2021;234:47–53.
46. Dickson RP, et al. Spatial variation in the healthy human lung microbiome and the adapted island model of lung biogeography. *Ann Am Thorac Soc*. 2015;12(6):821–830.
47. Dickson RP, et al. Towards an ecology of the lung: new conceptual models of pulmonary microbiology and pneumonia pathogenesis. *Lancet Respir Med*. 2014;2(3):238–246.
48. Peteranderl C, Herold S. The impact of the interferon/TNF-related apoptosis-inducing ligand signaling axis on disease progression in respiratory viral infection and beyond. *Front Immunol*. 2017;8:313.
49. Mueller C, et al. Lack of cystic fibrosis transmembrane conductance regulator in CD3+ lymphocytes leads to aberrant cytokine secretion and hyperinflammatory adaptive immune responses. *Am J Respir Cell Mol Biol*. 2011;44(6):922–929.
50. Xia W, et al. Interleukin-17A promotes MUC5AC expression and goblet cell hyperplasia in nasal polyps via the Act1-mediated pathway. *PLoS One*. 2014;9(6):e98915.
51. Peters-Hall JR, et al. Quantitative proteomics reveals an altered cystic fibrosis in vitro bronchial epithelial secretome. *Am J Respir Cell Mol Biol*. 2015;53(1):22–32.
52. Sass LA, et al. Complement effectors of inflammation in cystic fibrosis lung fluid correlate with clinical measures of disease. *PLoS One*. 2015;10(12):e0144723.
53. Fick RB Jr., et al. Complement activation in cystic fibrosis respiratory fluids: in vivo and in vitro generation of C5a and chemotactic activity. *Pediatr Res*. 1986;20(12):1258–1268.
54. Gharib SA, et al. Mapping the lung proteome in cystic fibrosis. *J Proteome Res*. 2009;8(6):3020–3028.
55. Keiser NW, et al. Defective innate immunity and hyperinflammation in newborn cystic fibrosis transmembrane conductance regulator-knockout ferret lungs. *Am J Respir Cell Mol Biol*. 2015;52(6):683–694.
56. Davies KE, et al. Cystic fibrosis is not caused by a defect in the gene coding for human complement C3. *Mol Biol Med*. 1983;1(2):185–190.
57. Holzhauer RJ, et al. Third component of complement in cystic fibrosis. *Am J Hum Genet*. 1976;28(6):602–606.
58. Lopes-Pacheco M. CFTR modulators: the changing face of cystic fibrosis in the era of precision medicine. *Front Pharmacol*. 2019;10:1662.